

Influence of CuO doping on cobalt oxide for thermochemical energy storage

Rongjun Wu ^a, Hongyu Huang ^b, Lisheng Deng ^b, Mitsuhiro Kubota ^a, Noriyuki Kobayashi ^{a,*}

^a Department of Chemical Systems Engineering, Graduate School of Engineering, Nagoya University, Furo-cho, Chikusa-ku, Nagoya-shi, Aichi, 464-8603, Japan

^b Guangzhou Institute of Energy Conversion, Chinese Academy of Sciences, No. 2 Nengyuan Road, Wushan, Tianhe District, Guangzhou, 510640, China



ARTICLE INFO

Keywords:

Thermochemical energy storage
Cobalt oxide
CuO doping
Reduction/re-oxidation behavior
Repeatability performance

ABSTRACT

Thermochemical energy storage (TCS) was considered as a promising candidate for renewable energy utilization and energy efficient utilization. Particularly, metal oxide-based TCS has attracted increasing attention due to its operation possibility with air. In this work, CuO-doped cobalt oxide composite was prepared by a simple mechanical mixing process and explored for TCS application. The influences of CuO doping on the redox behavior, repeatability and the optical absorption property of cobalt oxide were investigated. Doping with CuO significantly decreased the onset temperature of reduction by 60 °C compared to pure cobalt oxide. Meanwhile, the result verifies that the onset temperature of re-oxidation could be tuned in the range from 825 to 890 °C by altering the doping amount of CuO. The reason for the tunable onset temperature was examined from the viewpoint of the structural transformation of the composite during the reduction/re-oxidation process. It was presumed that the doping amount of Cu species in CoO might relate to the onset temperature of re-oxidation. The repeatability of the composite was highly affected by the doping amount of CuO. Moreover, CuO with relatively small particle size exhibited a positive effect on improving the repeatability of CuO-doped cobalt oxide composite. Additionally, the absorption spectra demonstrate that CuO doping would affect the optical absorption property of the composite, enhancing the absorption of visible light. Hence, the results obtained in this work indicate that doping with CuO could be a promising method to extend the applicability of cobalt oxide-based system for TCS application.

1. Introduction

As fossil fuel energy consumption and CO₂ emission are mounting up year by year, renewable energy utilization and energy efficient utilization are increasingly becoming vital subjects in the world. Solar energy, as an abundant and clean renewable energy, is expected to play a significant role in the further. A crucial challenge for solar energy utilization now is how to store the solar energy [1,2]. Typically, solar thermal energy which is a major form of harnessing solar energy can be stored by means of sensible heat storage, latent heat storage and thermochemical energy storage technologies [2,3]. Thermochemical energy storage (TCS) technology, which can store and release thermal energy by reversible chemical reactions, possesses the following prominent advantages [2,4]: high thermal energy storage capacity, large working temperature range, long-term storage period and long transport possibility in comparison with the other two thermal energy storage technologies. There are several types of TCS systems based on different chemical reactions such as hydration/dehydration system [5–7] (e.g.

LiOH/LiOH·H₂O, CaO/Ca(OH)₂ and MgO/Mg(OH)₂), carbonation/decarbonation system [8,9] (e.g. CaO/CaCO₃, SrO/SrCO₃), reduction/oxidation system [10] (e.g. Co₃O₄/CoO and Mn₂O₃/Mn₃O₄) and so on. In recent years, metal oxide-based TCS system, which is based on reduction and oxidation of metal oxides, has attracted increasing attention in concentrating solar power plants due to its high working temperature and convenient operation with air. High temperature air heated by solar radiation can be used to trigger the reduction of metal oxide, simultaneously partial thermal energy will be stored in the reduced metal oxide. In the off-sun period, the thermal energy can be released by oxidizing the metal oxide with air. Air is utilized as oxygen source and heat transfer fluid. Theoretically, this system can be performed in an open-loop system that there are no technical requirements for gas separation and gas storage [2,10,11].

Currently, researches on metal oxide-based TCS system were mainly at lab-scale. A research focus was the development of suitable energy storage materials. Several conventional metal oxides were studied and discussed. BaO/Ba₂O [12,13], Mn₂O₃/Mn₃O₄ [14], Co₃O₄/CoO [15]

* Corresponding author. Nagoya University, Furo-cho, Chikusa-ku, Nagoya-shi, Aichi, 464-8603, Japan.

E-mail address: kobayashi.noriyuki@material.nagoya-u.ac.jp (N. Kobayashi).

and CuO/Cu₂O [16] were proposed as the promising candidates for metal oxide-based TCS application. Additionally, novel materials like perovskite oxides [17–19] and many multi-metal oxides like iron-doped manganese oxides, lithium-manganese oxides, copper-manganese oxides [20–22] were synthesized and assessed. Meanwhile, gram-scale [23,24] and kilogram-scale [25,26] experiments for metal oxide-based TCS system were growing faster with the advances on materials. Cobalt oxide (i.e. Co₃O₄/CoO) was considered as the most attractive candidate for metal oxide-based TCS application owing to its remarkable reaction repeatability and high energy storage density (844 kJ/kg) [10, 15,27]. The relevant redox reaction equation is shown below:



Masses of researches based on cobalt oxide were developed. Pure cobalt oxide has been further explored on maximizing the amount and optimizing the shape for the exploitation in various reactor concepts [28,29]. Significantly, cobalt oxide system has been tested at pilot-plant scale (90 kg) in Solar Tower Julich (Germany) [25]. Meanwhile, due to the high reaction temperature of cobalt oxide (~900 °C), which will limit the possible applications not only in concentrating solar power plants but also in other applications such as industrial waste heat recovery, cobalt oxide was modified by doping with several metal components (e.g. Fe, Mn, Ni, Cu and Mg) to improve the chemical parameters and lower the working temperature [15,30–34]. Portilla-Nieto et al. [34] synthesized Co_{3-x}Ni_xO₄ materials by means of sol-gel method. They reported that doping with Ni significantly decreased the reduction and oxidation temperatures. Similarly, Block et al. [32] prepared copper oxide/cobalt oxide systems by sol-gel method. The result revealed a decreased working temperature by doping with Cu. In addition, they reported that the cobalt-rich compositions with 0.1 ≤ x ≤ 0.33 (x was the molar ratio of Cu/(Cu + Co)) showed fast kinetics. While Agrafiotis et al. [15] proposed that CuCo₂O₄ in which the molar ratio of Cu/(Cu + Co) was 0.33 showed a slow re-oxidation rate in the first cycle. The different repeatability behaviors of Cu-doped cobalt oxide systems in literatures appeared to need a deeper investigation. It was found that the morphological changes might affect the oxygen mass transfer in re-oxidation process [10]. Also, Carrillo et al. [14] have reported that the morphological change influenced the repeatability of Mn₂O₃/Mn₃O₄ pairs. They concluded that different sintering mechanisms, which depended on the particle size of the material in that work, induced different morphological evolutions. Similar to Mn₂O₃/Mn₃O₄ system, Cu-doped cobalt oxide system also underwent a thermal sintering process at high temperature during the reduction-oxidation processes [32]. Hence, the investigation of the effect of morphology evolution on the repeatability performance of Cu-doped cobalt oxide is of great interest.

The aim of this work is to extend more possibility of cobalt oxide-based materials for TCS application. In this work, copper component was also considered as the dopant for cobalt oxide-based TCS system. We proposed a copper oxide (CuO)-doped cobalt oxide composite. The composite was prepared by mechanically mixing CuO and Co₃O₄ powders at room temperature. An in-depth investigation on the influences of CuO doping on the redox behavior and the repeatability performance of cobalt oxide-based TCS system was proceeded. In addition, the effect of the particle size of CuO on the repeatability performance was also explored. In view of the results reported in literatures, different particle sizes of metal oxides (e.g. Mn₂O₃ and ZrO₂) were prepared by precipitation method with different precursor concentrations [14,35]. Precipitation method was also utilized as a facile way to obtain CuO nanoparticles [36]. Thereby, precipitation method using different copper nitrate concentrations was employed in the present work to synthesize CuO with different particle sizes.

2. Experimental section

2.1. Materials preparation

2.1.1. Preparation of CuO

Precipitation method was employed to synthesize CuO powder [36]. Precursor solutions of Cu(NO₃)₂·2H₂O (99.9%, Kanto Chemical CO., INC.) were prepared with deionized water. The concentrations of the copper nitrate solution were varied in the range between 0.025 and 0.5 M. After stirring at room temperature for 30 min, 1 M sodium hydroxide (97.0%, Kanto Chemical CO., INC.) was added drop-wise with constant stirring. The addition of sodium hydroxide was finished when the solution was in excess to a pH of 11 ± 1. The resulting precipitate was aged and stirred for 24 h. Then, the obtained precipitate was filtered and washed with deionized water seven times and dried at 80 °C overnight. Afterwards, the solid was calcined at 700 °C for 4 h with a heating rate of 2 °C/min. The obtained CuO samples prepared with copper nitrate concentration of 0.025 M, 0.05 M, 0.1 M and 0.5 M were labeled as CuO (0.025 M), CuO (0.05 M), CuO (0.1 M) and CuO (0.5 M), respectively.

2.1.2. Preparation of CuO-doped cobalt oxide composite

Co₃O₄ powder (99.99%, Kanto Chemical CO., INC.) was used as received. Certain amount of Co₃O₄ and CuO were weighed and put in a mortar. To avoid the deviation generated in the milling process, the total weight of each sample was weighed in ~1000 mg. Materials were carefully mixed by hand, grinding with a speed of ~2 laps per second for 20 min. In the present work, composites doped with different CuO contents were prepared. The CuO content, x, is defined as,

$$x = \frac{m_{\text{CuO}}/\text{M}_{\text{CuO}}}{m_{\text{CuO}}/\text{M}_{\text{CuO}} + m_{\text{Co}_3\text{O}_4}/\text{M}_{\text{Co}_3\text{O}_4}} \quad (2)$$

where m_{CuO} is the weight of CuO, M_{CuO} is the molar mass of CuO, $m_{\text{Co}_3\text{O}_4}$ is the weight of Co₃O₄, and $\text{M}_{\text{Co}_3\text{O}_4}$ is the molar mass of Co₃O₄.

2.2. Materials characterization

X-ray diffraction (XRD; Rigaku Ultima IV) with Cu K α radiation (40 kV/30 mA) was employed to identify the crystal phases of samples. The cell parameters of CoO phases of samples were derived from (111) (200) (220) facets, basing on Bragg's law.

Scanning electron microscope (SEM; JEOL JSM-7500FA) was exploited to appreciate the morphologies of samples. ImageJ software was used in this study to obtain the particle size distributions of samples by statistical analysis of SEM image. More than 300 particles were analyzed for each sample.

Surface area and pore size distribution analyzer (BELSORP MAX II) with the multi-point BET method was utilized to obtain the specific surface area (S_{BET}) values of CuO samples.

In-situ X-ray diffraction (in-situ XRD; Rigaku SmartLab 3 kW) with Cu K α radiation (40 kV/40 mA) was operated to detect the structural transformations of samples during the reduction/re-oxidation steps. Samples were detected in a heating-cooling cycle between 30 °C and 950 °C under air atmosphere.

Thermogravimetric analyzer (TGA; HITACHI STA7300) was carried out with samples weight of ~10 mg. Typically, the temperature program for one reduction-oxidation cycle consisted of a heating step from 700 °C to 1000 °C with dwell time of 5 min and a cooling step from 1000 °C to 700 °C with dwell time of 5 min. Each sample was tested at a heating/cooling rate of 10 °C/min under air atmosphere with a constant flow of 200 mL/min. During the reduction process, oxygen released, leading to a weight loss for the sample. During re-oxidation process, oxygen uptake occurred, leading to a weight gain for the sample. The weight change, α (%), is defined as,

$$\alpha = \frac{m_i - m_f}{m_i} \times 100 \quad (3)$$

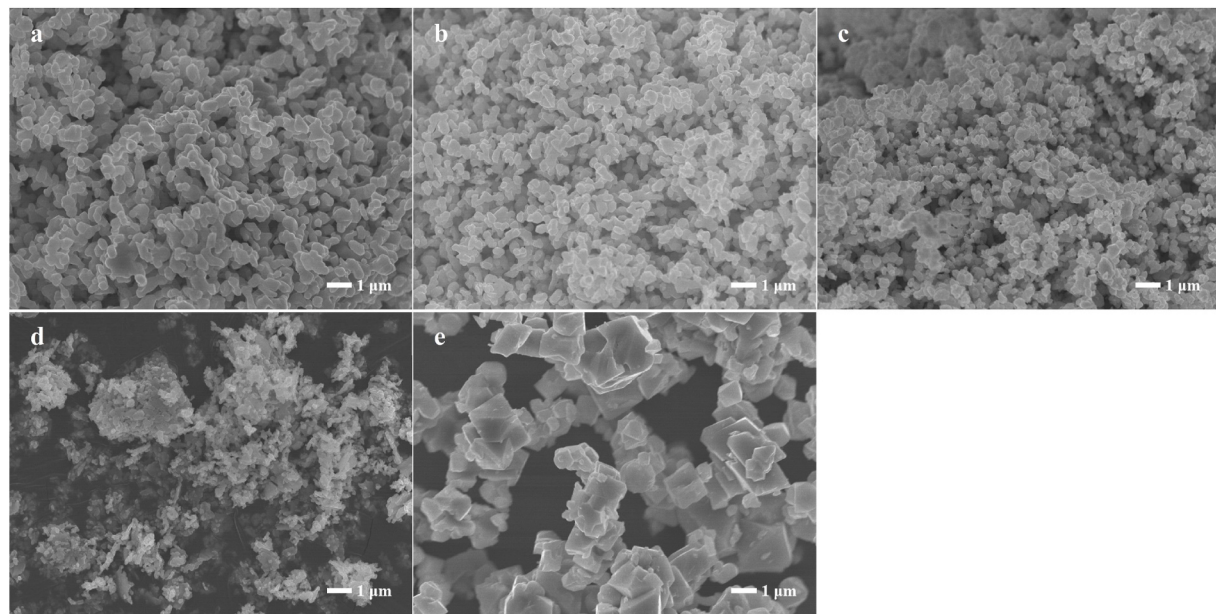


Fig. 1. SEM images of samples: (a) CuO (0.5 M), (b) CuO (0.1 M), (c) CuO (0.05 M), (d) CuO (0.025 M), and (e) pure Co₃O₄.

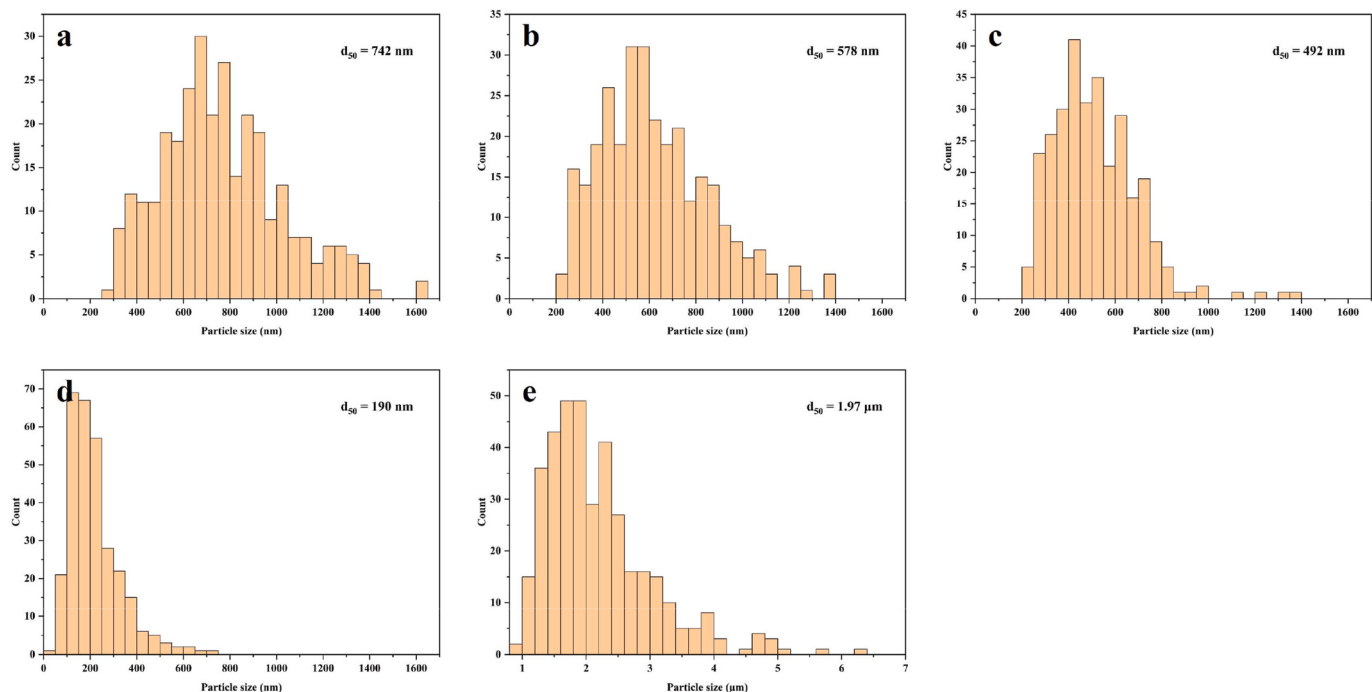


Fig. 2. Particle size distribution histograms of samples: (a) CuO (0.5 M), (b) CuO (0.1 M), (c) CuO (0.05 M), (d) CuO (0.025 M) and (e) pure Co₃O₄.

Table 1

Specific surface area (S_{BET}) values of CuO samples prepared with different copper nitrate concentrations.

Sample name	Concentration (M)	S _{BET} (m ² /g)
CuO (0.5 M)	0.5	2.01
CuO (0.1 M)	0.1	2.58
CuO (0.05 M)	0.05	2.71
CuO (0.025 M)	0.025	6.08

where m_i is the initial weight of sample, and m_t is the weight at time t . Due to the possible impurities existed in samples, initial weight of the second cycle was determined as the initial weight for each sample.

Moreover, the conversion ratio of reduction/re-oxidation, β , is defined as,

$$\beta = \frac{|m_0 - m_t|}{|m_i - m_f|} \quad (4)$$

where m_0 is the weight of sample at the beginning of the reduction/re-oxidation process, m_t is the weight at time t , and m_f is the final weight of sample after the reduction in the second cycle.

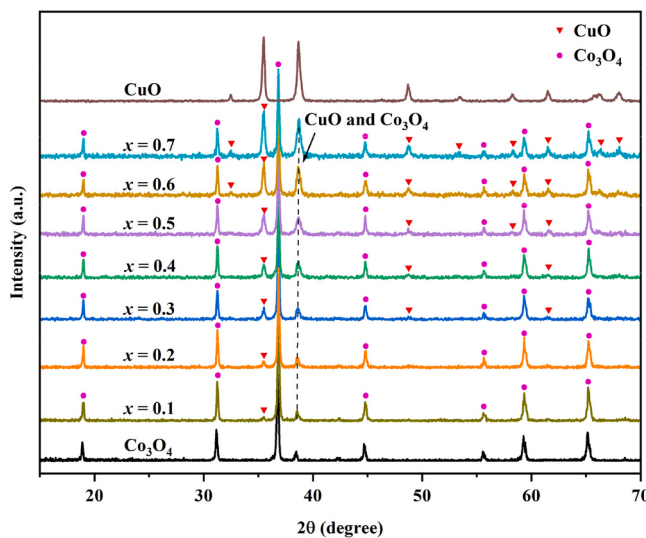


Fig. 3. XRD patterns of pure Co₃O₄, pure CuO (0.5 M) and composites doped with different CuO (0.5 M) contents (x).

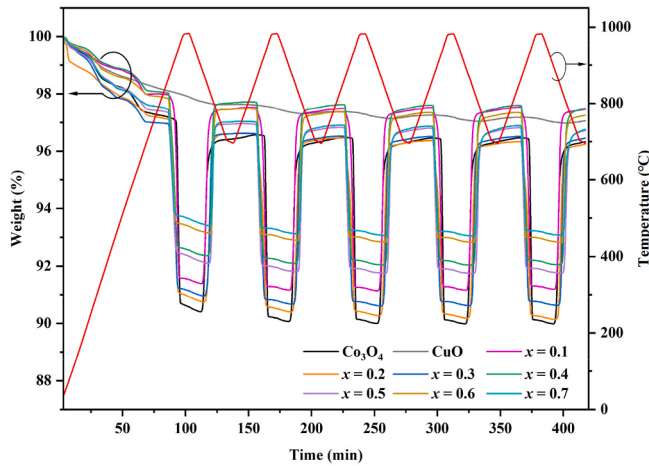


Fig. 4. TGA curves of pure Co₃O₄, pure CuO (0.5 M) and composites with different CuO (0.5 M) contents (x).

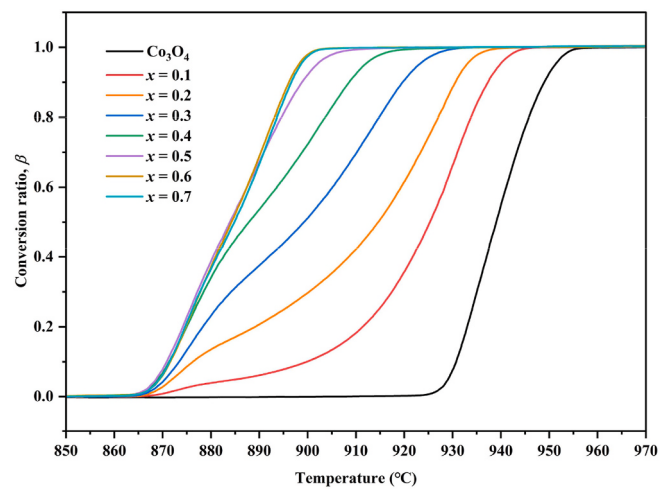


Fig. 5. Evolutions of reduction conversion for Co₃O₄ and composites with different CuO (0.5 M) contents (x).

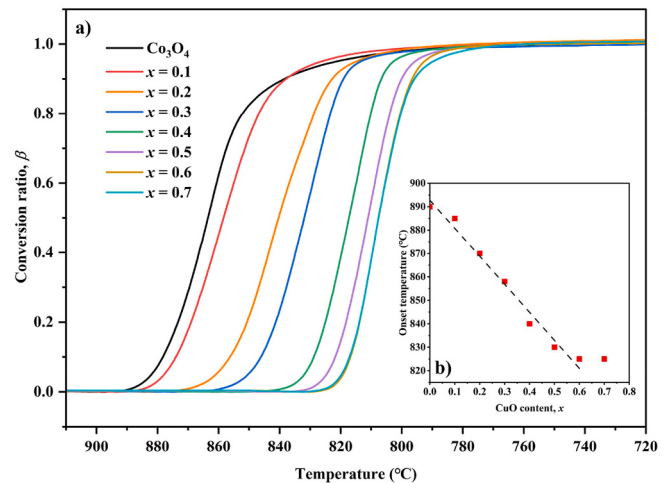


Fig. 6. (a) Evolutions of re-oxidation conversion for cobalt oxide and composites with different CuO (0.5 M) contents (x) and (b) Evolution of the onset re-oxidation temperature as a function of CuO content (x).

Table 2

Onset temperature of reduction/re-oxidation, weight loss (α), reaction time and charging/discharging heat for pure cobalt oxide and composites doped with different CuO contents (x).

Sample	^{a, b} T _{onset red} (°C)	^{a, b} T _{onset oxi} (°C)	^a Weight loss (%)	^a Reduction time (min)	^a Re-oxidation time (min)	^a Charging heat (kJ/kg)	^a Discharging heat (kJ/kg)
CuO (0.5 M), $x = 0$	925	890	6.5	3.3	11.2	541	494
CuO (0.5 M), $x = 0.1$	865	885	6.4	8.1	9.0	527	472
CuO (0.5 M), $x = 0.2$	865	870	6.2	7.6	7.6	505	457
CuO (0.5 M), $x = 0.3$	865	858	6.0	6.7	6.3	501	422
CuO (0.5 M), $x = 0.4$	865	840	5.6	5.8	5.6	446	436
CuO (0.5 M), $x = 0.5$	865	830	5.1	5.0	5.1	423	403
CuO (0.5 M), $x = 0.6$	865	825	4.5	3.4	4.6	346	317
CuO (0.5 M), $x = 0.7$	865	825	3.8	3.4	5.2	317	289
CuO (0.1 M), $x = 0.6$	865	825	4.6	3.5	4.6	350	328
CuO (0.05 M), $x = 0.6$	865	825	4.5	3.4	4.5	349	316
CuO (0.025 M), $x = 0.6$	865	825	4.5	3.4	4.6	345	323

^a The data was based on the second cycle.

^b The onset temperature in this work corresponds to the start temperature of sharp weight change under the configured temperature program.

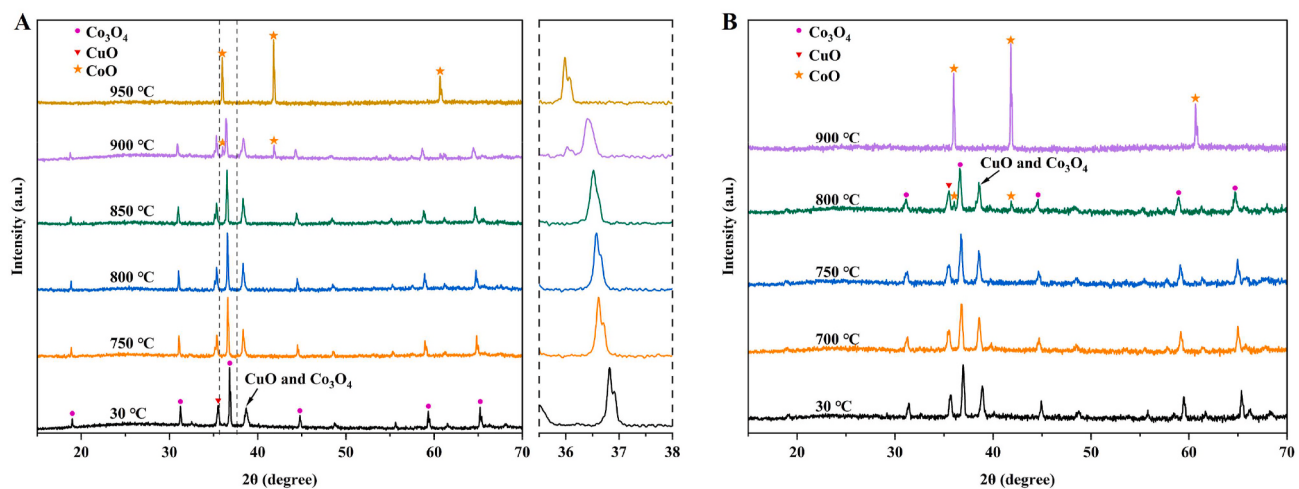


Fig. 7. In-situ XRD patterns of composite with CuO (0.5 M) content of $x = 0.6$: (A) In the heating step. The dashed-line zone was showed in the right panel. (B) In the cooling step.

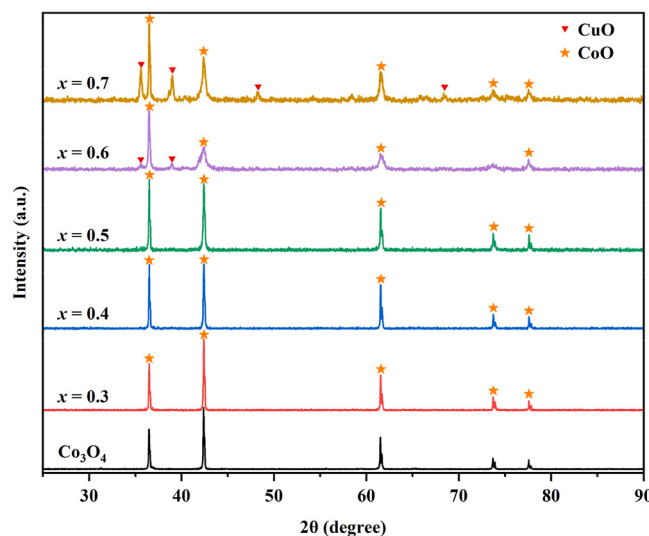


Fig. 8. XRD patterns of reduced pure cobalt oxide and composites with different CuO (0.5 M) contents (x).

The charging-discharging heat values of samples during the reduction-oxidation processes were collected by a simultaneous TGA-DSC thermal analysis system (TGA/DSC; METTLER TOLEDO TGA/DSC 3+). Samples were tested under air atmosphere with a constant flow of 100 mL/min. The heating and cooling steps were proceeded under the ramping rates of ± 10 °C/min.

In addition, the optical absorption properties of samples were measured by a UV-Visible-NIR-Spectrophotometer (PerkinElmer Lambda 750) in the wavelength range from 300 to 2000 nm.

3. Results and discussion

The XRD result shown in Fig. S1 illustrates that all the CuO samples prepared by precipitation method presented the characteristic reflections of CuO phase (PDF#01-080-1268). Fig. 1a-d show the SEM images of the CuO samples prepared with different copper nitrate concentrations. As we can observe, all the CuO samples presented agglomerate morphologies which were formed by similar irregular shape particles. Meanwhile, it is possible to appreciate that the CuO samples prepared with different copper nitrate concentrations exhibited different particle sizes. The CuO sample prepared with a lower

concentration presented a relatively small particle size. This fact can be observed more clearly by the particle size distributions shown in Fig. 2. By lowering the copper nitrate concentration, the particle size distribution of the as-prepared CuO sample narrowed and shifted toward smaller diameter. Moreover, the S_{BET} values (Table 1) of the CuO samples increased from $2.01 \text{ m}^2/\text{g}$ to $6.08 \text{ m}^2/\text{g}$ when the copper nitrate concentrations decreased from 0.5 M to 0.025 M. In short, the results indicate that the concentration of copper nitrate solution affected the particle size of as-prepared CuO powder. In addition, the morphology and the particle size distribution of pure Co_3O_4 were displayed in the Figs. 1e and 2e, respectively. Pure Co_3O_4 also presented an agglomerate morphology, which is the common characteristic of metal oxide powders. Moreover, pure Co_3O_4 exhibited a relatively large particle size distribution by comparing with the CuO samples.

Fig. 3 displays the XRD patterns of pure Co_3O_4 , pure CuO (0.5 M), and CuO-doped cobalt oxide composites with different CuO (0.5 M) contents (x). The result confirms that each composite exhibited Co_3O_4 phase (PDF#00-043-1003) and CuO phase (PDF#01-080-1268). Furthermore, the higher the CuO content doped in the composite was, the more intense the CuO diffractions presented.

The redox behaviors of samples were performed by TGA in five reduction-oxidation cycles between 700 °C and 1000 °C. CuO (0.5 M) was used as the dopant to prepare the CuO-doped cobalt oxide composite. The effect of CuO doping on the redox behavior of cobalt oxide was explored. For comparison, pure Co_3O_4 and pure CuO (0.5 M) were also tested under the same condition. As shown in Fig. 4, there was a continuous weight loss in the first heating step for each sample, which may be caused by the removal of some adsorbed compounds like water and CO_2 [14,31]. Afterwards, there was no sharp weight loss and weight gain occurred for pure CuO (0.5 M) between 700 °C and 1000 °C. As described in the introduction, CuO/ Cu_2O was also considered as a promising candidate for metal oxide-based TCS application. However, the onset reduction temperature of CuO to Cu_2O was higher than 1000 °C [16], which accounts for the result shown in Fig. 4. Conversely, rapid weight loss in the heating step which was attributed to the reduction process and rapid weight recovery in the subsequent cooling step which was attributed to the re-oxidation process can be observed for pure Co_3O_4 and the composites doped with CuO (0.5 M). Additionally, with an increase in CuO (0.5 M) content (x), there was a decrease in the weight change (Table 2). The reason is that the reactive component (i.e. cobalt oxide) content in the composite decreased as the CuO content increased, resulting in a decrease in the oxygen release/uptake amount during the reduction/oxidation process. It should be noted that this fact would affect the heat storage and release capacities of the composites

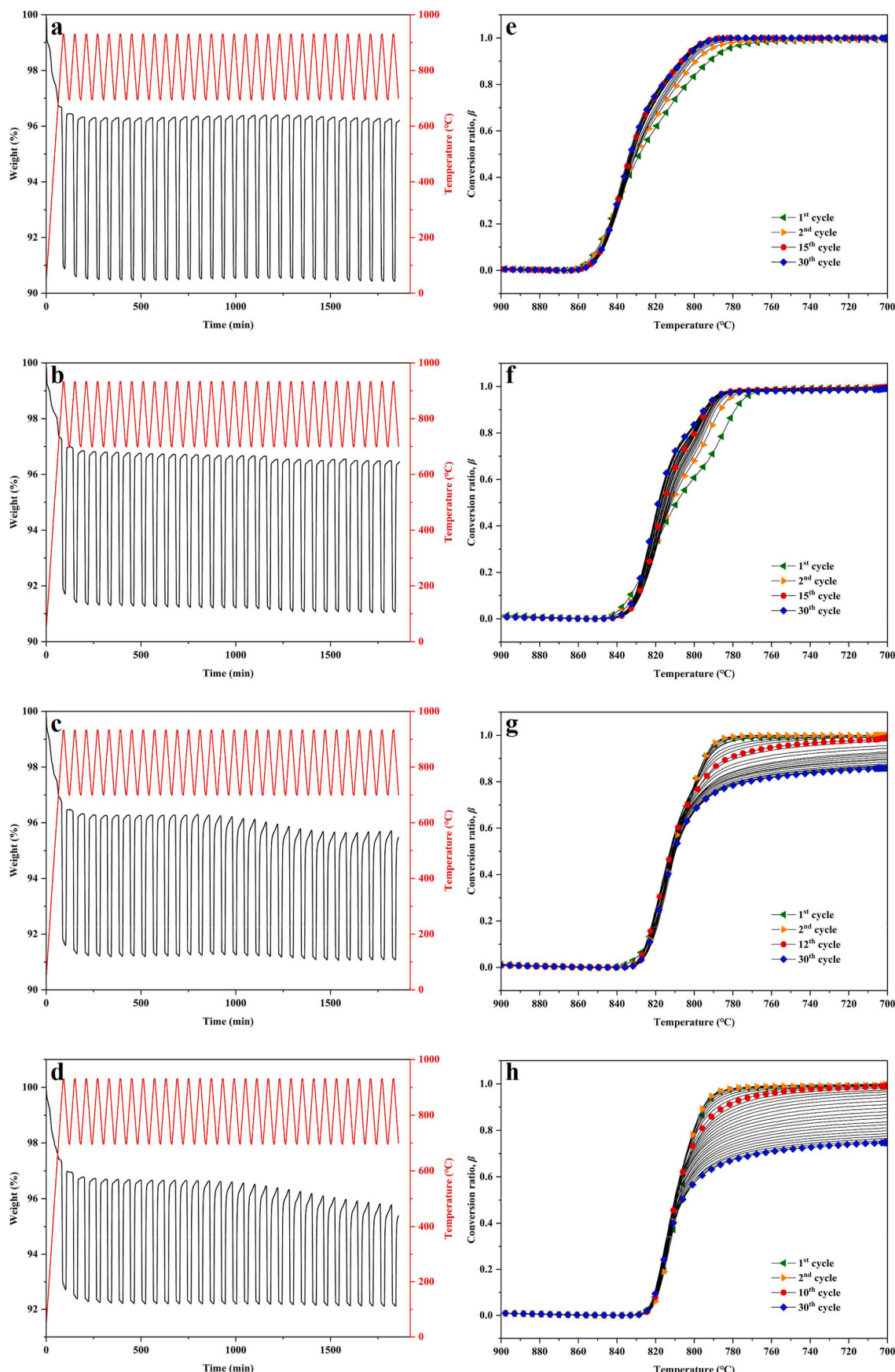


Fig. 9. TGA curves and evolutions of re-oxidation conversion in 30 reduction-oxidation cycles for composites doped with different CuO (0.5 M) contents (x): (a and e) $x = 0.3$, (b and f) $x = 0.4$, (c and g) $x = 0.5$, and (d and h) $x = 0.6$.

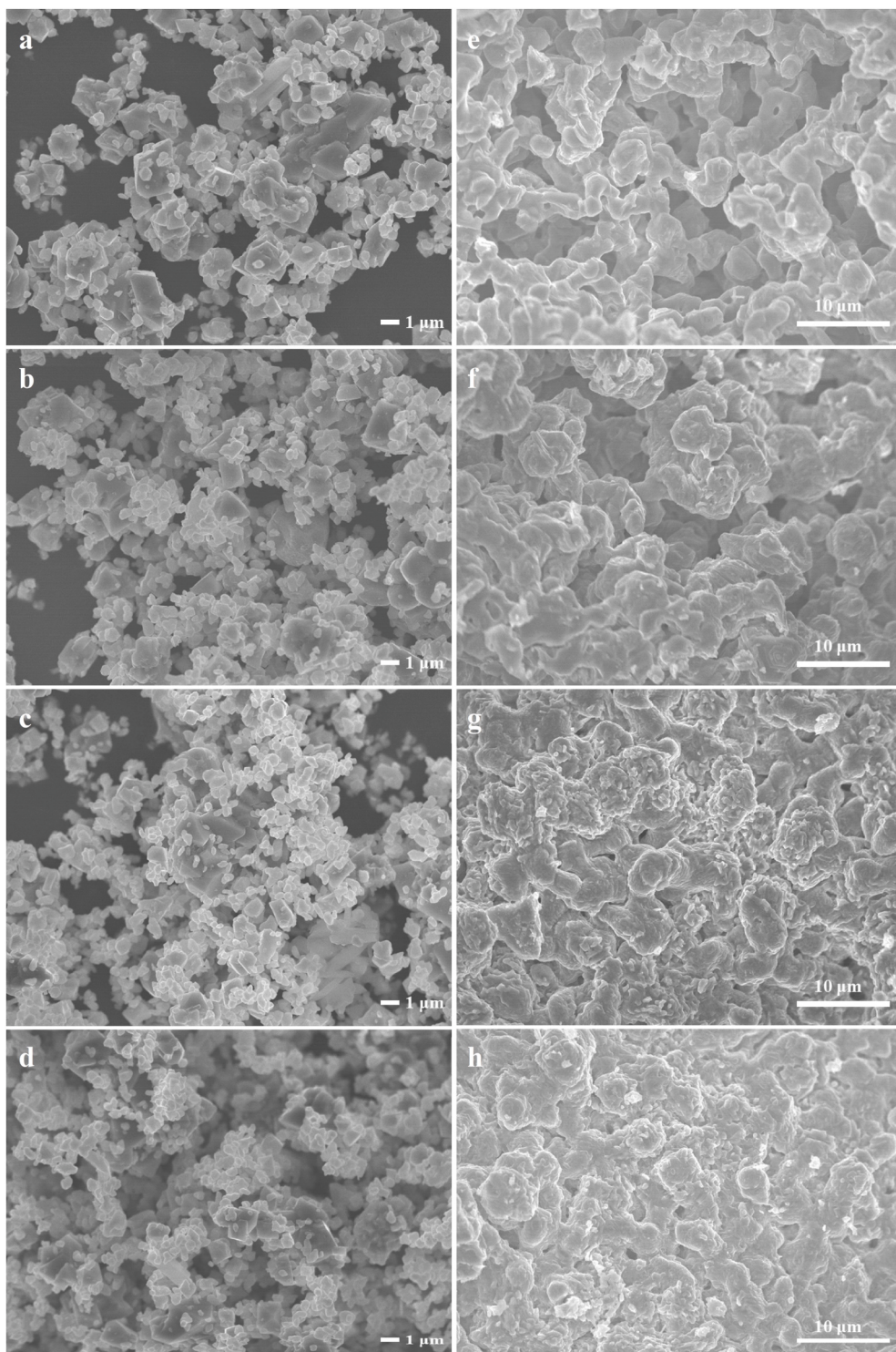


Fig. 10. SEM images taken before and after 30 cycles for composites doped with different CuO (0.5 M) contents (x): (a and e) $x = 0.3$, (b and f) $x = 0.4$, (c and g) $x = 0.5$, and (d and h) $x = 0.6$.

[33]. The charging-discharging heat values during the reduction-oxidation processes for the samples were collected by DSC. A typical TGA-DSC analysis is displayed in Fig. S2. As shown in Table 2, the charging/discharging heat decreased with the increasing content of CuO, which is in accordance with the work of Block et al. [32]. Meanwhile, the discharging heat was lower than the corresponding charging heat, which might be due to the relatively slow re-oxidation rate as well as the heat loss caused by using the open alumina crucibles in DSC.

Fig. 5 displays the evolutions of reduction conversion in the second cycle for pure Co_3O_4 and the composites with different CuO (0.5 M) contents (x). With the increasing of temperature, the conversion ratio of each sample increased. As we can see, doping with CuO shifted the onset reduction temperature from 925 °C for pure Co_3O_4 to 865 °C for the CuO-doped composites. All the composites exhibited the same onset reduction temperature while presented different reduction rates. As shown in Table 2, pure Co_3O_4 took ~3.3 min to complete the reduction,

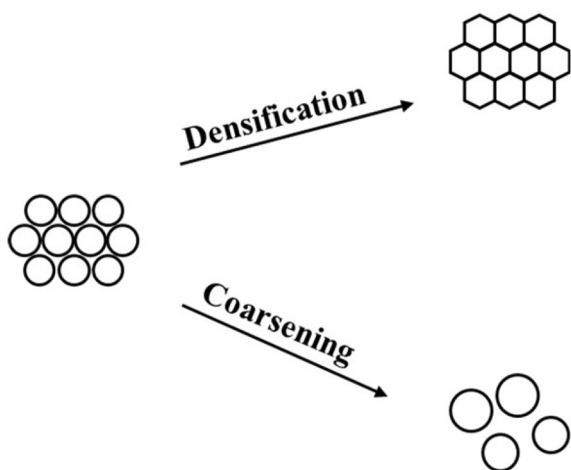


Fig. 11. Schematic of two possible phenomena during solid state sintering process [14].

whereas the composite doped with CuO (0.5 M) content of $x = 0.1$ finished the reduction in ~ 8.1 min. It can be observed that increasing the CuO (0.5 M) content (x) from 0.1 to 0.6 improved the reduction rate gradually. Eventually, the curves for the composites doped with CuO (0.5 M) content of $x \geq 0.6$ were nearly identical. It took ~ 3.4 min to obtain complete reduction.

Fig. 6a describes the evolutions of re-oxidation conversion in the second cycle for pure cobalt oxide and the composites with different CuO (0.5 M) contents (x). As shown in Fig. 6a, doping with CuO lowered the re-oxidation temperature apparently. Furthermore, increasing CuO content linearly decreased the onset re-oxidation temperature from 890 °C for pure cobalt oxide to 825 °C for the composite doped with CuO (0.5 M) content of $x = 0.6$ (Fig. 6b). When the CuO (0.5 M) content (x) exceeded 0.6, there was no significant shift for the onset temperature of re-oxidation. In addition, the composites doped with different CuO (0.5 M) contents (x) exhibited an increase in the re-oxidation rate in the second cycle, as shown in Table 2. In a word, doping with CuO diminished the onset temperatures of reduction and re-oxidation of cobalt oxide. Moreover, it is possible to tune the onset re-oxidation temperature in the range from 825 °C to 890 °C by adjusting the CuO content in the composite.

To study the reduction/re-oxidation process of CuO-doped cobalt oxide composite, the structural transformation under a heating-cooling cycle for the composite doped with CuO (0.5 M) content of $x = 0.6$ was detected by in-situ XRD. As shown in Fig. 7A, the characteristic diffraction patterns of Co_3O_4 phase (PDF#00-043-1003) and CuO phase (PDF#01-080-1268) can be observed for the composite at room temperature. As the temperature increased, there was a slight shift in the diffraction peaks toward smaller angle, which might be caused by the thermal expansion [37]. Meanwhile, the intensities of Co_3O_4 and CuO patterns decreased. Eventually, no Co_3O_4 phase and CuO phase were detected at 950 °C while a single phase of CoO (PDF#00-043-1004) presented, attributing to the reduction process. Afterwards, as shown in Fig. 7B, Co_3O_4 phase and CuO phase reappeared while CoO phase disappeared as the temperature decreased to room temperature in the cooling step, attributing to the re-oxidation process. The result confirms the structural transformation of cobalt oxide during the reduction/re-oxidation process. Significantly, it was found that CuO was involved in the process. Cu species might dope into CoO structure during the reduction process and separate out during the re-oxidation process.

Moreover, Fig. 8 displays the XRD patterns of reduced pure cobalt oxide and the composites with different CuO (0.5 M) contents (x). These reduced samples were obtained by heating the samples to 1000 °C in air and then cooling the samples from 1000 °C to room temperature under nitrogen atmosphere. The result confirms the presence of CoO (PDF#00-

043-1004) in all the samples, which was produced by the reduction of Co_3O_4 . It is worth noting that a secondary phase corresponding to CuO (PDF#01-080-1268) was detected for the composites with CuO (0.5 M) content of $x \geq 0.6$. However, no CuO phase was detected for the composite with $x = 0.6$ at 950 °C (as shown in Fig. 7). The cell parameters of these two CoO phases were calculated, basing on Bragg's law. The result shows that the cell parameter of CoO phase for the composite with $x = 0.6$ at 950 °C was 4.31 Å while the cell parameter of the CoO phase at room temperature was 4.26 Å. Thus, the expanded CoO crystal caused by thermal expansion at high temperature might allow more Cu species to dope into CoO crystal, leading to no CuO phase detected by XRD. In short, the result indicates that the doping amount of Cu species in CoO crystal was limited. This might explain the result illustrated in Fig. 6 that the onset temperature of re-oxidation decreased gradually with the increasing amount of Cu species in CoO crystal. We presumed the Cu species doped in CoO was beneficial to decrease the onset temperature of re-oxidation. However, a deeper investigation is necessary and needed in the future.

The repeatability and stability of energy storage materials are of particular importance for TCS application. Hence, CuO (0.5 M)-doped cobalt oxide composites and pure cobalt oxide were subjected to 30 reduction-oxidation cycles with a heating/cooling rate of 10 °C/min. Consistent with the results reported in literatures [10,15,27], pure cobalt oxide exhibited a stable repeatability behavior (Fig. S3). Fig. 9 shows the TGA curves and the evolutions of re-oxidation conversion in 30 cycles for the composites doped with different CuO (0.5 M) contents (x). As we can see clearly, when the CuO (0.5 M) content was $x = 0.3$ and 0.4, the composites presented stable repeatability performances in 30 reduction-oxidation cycles, reaching a complete re-oxidation conversion in each cycle. In addition, as the reduction-oxidation cycle proceeded, the re-oxidation rate improved slightly. However, in the case of the composites with $x \geq 0.5$, the weight change decreased gradually during the cycles. Apparently, the composite with CuO (0.5 M) content of $x \geq 0.5$ suffered a decline of re-oxidation rate in the 30 cycles, resulting in an insufficient re-oxidation time. The weight loss for the composite with $x = 0.5$ did not recover completely in the cooling step from the 12th cycle. Ultimately, $\beta = 0.89$ of re-oxidation conversion obtained after the temperature decreased from 950 °C to 700 °C in the 30th cycle. Likewise, incomplete re-oxidation in the cooling step took place from the 10th cycle for the composite with CuO (0.5 M) content of $x = 0.6$, resulting in a re-oxidation conversion of $\beta = 0.75$ after the cooling step of the 30th cycle. These results clarify that the CuO content was associated with the repeatability performance of the CuO-doped cobalt oxide system.

Fig. 10 shows the SEM images taken before and after the 30 cycles for the composites doped with different CuO (0.5 M) contents (x). The particle size of the employed Co_3O_4 was relatively large compared to the CuO particles in this work. Thus, it is possible to observe from the SEM images of the fresh composites that CuO particles dispersed on the surface of Co_3O_4 particles. Also, agglomerate morphologies could be appreciated for all the fresh composites. While the morphologies changed dramatically after the 30 cycles owing to sintering effect. Typical necks were formed between inter-particles for all the composites after the 30 cycles. It can be appreciated that the composites with CuO (0.5 M) content of $x = 0.3$ and 0.4 presented coral-like array morphologies with large open pores, which were similar to the morphology of pure cobalt oxide after the 30 cycles (Fig. S3). Furthermore, no CuO particles could be distinguished from the bulk. For the composites with CuO (0.5 M) content of $x \geq 0.5$, non-uniform morphologies with less voids were exhibited. Meanwhile, several particles still could be appreciated on the surface of the bulk after the 30 cycles. B. Wong et al. have pointed out that the decreasing of re-oxidation conversion over cycling might relate to the morphological changes which affected the oxygen mass transfer [10]. Thereby, the different morphologies of the composites shown in Fig. 10 might explain the different repeatability performances of the composites. The large pores in the composites with

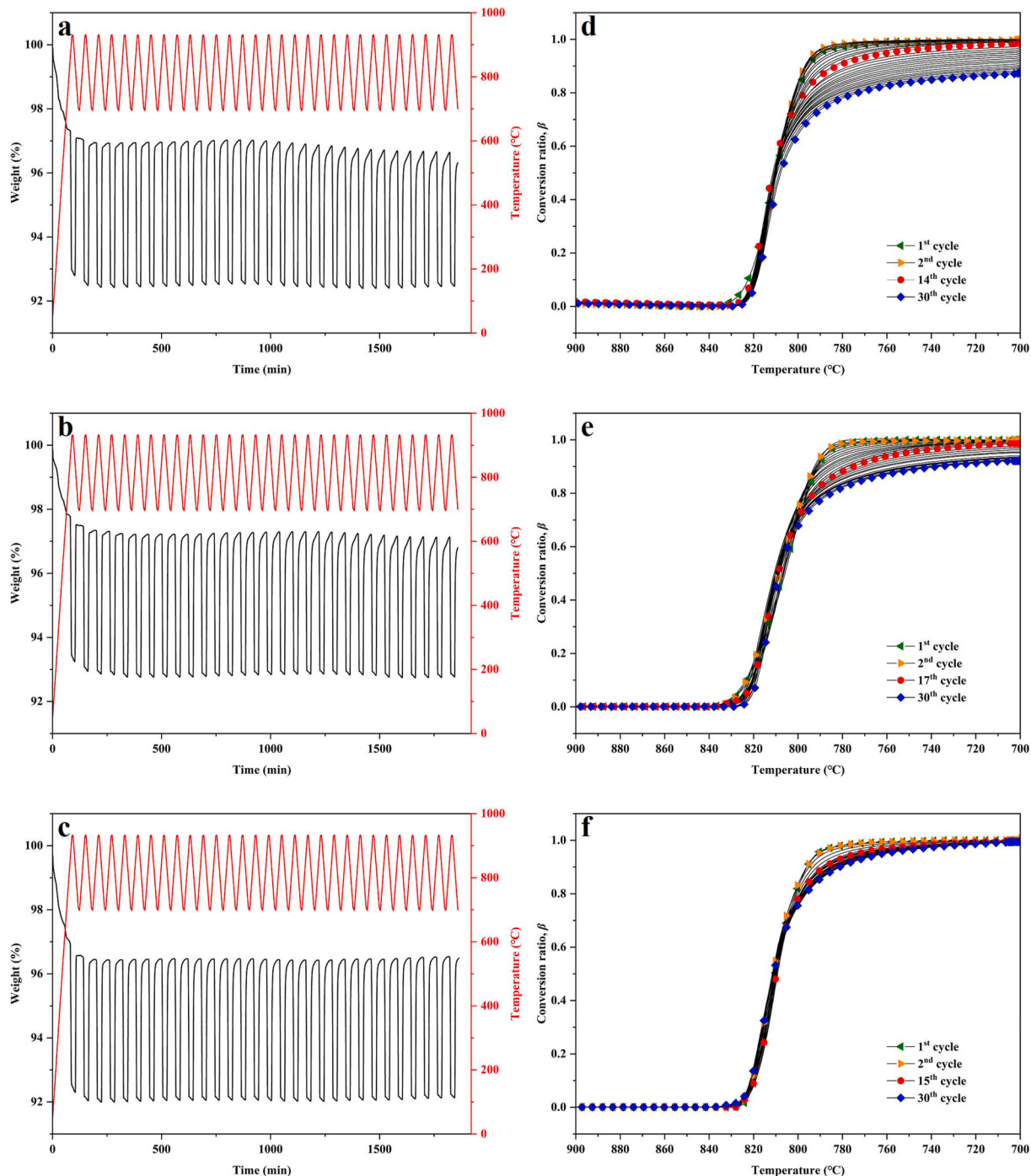


Fig. 12. TGA curves and evolutions of re-oxidation conversion in 30 reduction-oxidation cycles for composites doped with CuO content of $x = 0.6$: (a and d) CuO (0.1 M)-doped composite, (b and e) CuO (0.05 M)-doped composite and (c and f) CuO (0.025 M)-doped composite.

CuO (0.5 M) content of $x = 0.3$ and 0.4 were beneficial for the oxygen diffusion, leading to the stable re-oxidation rate and the excellent repeatability. Whereas the relatively dense morphologies presented in the composites with CuO (0.5 M) content of $x \geq 0.5$ hindered the oxygen diffusion, leading to the low re-oxidation rate and the deterioration in repeatability. It is reasonable to infer that CuO doping somehow affected the sintering process of cobalt oxide which caused different morphological changes, leading to different reduction-oxidation repeatability behaviors.

It is generally well known that solid state sintering is accompanied by coarsening and densification phenomena (Fig. 11). These two phenomena are usually in competition. When the sintering process is

dominated by densification, the voids among contacting particles become smaller and disappear and the material shrinks, whereas when the sintering process is dominated by coarsening, the particles grow by consuming the neighboring particles and the voids among particles become larger [38–40]. Accordingly, as shown in Fig. 10, the increasing content of CuO might promote the densification process, contributing to the elimination of voids among particles.

To further investigate the effect of CuO doping on the morphology evolution and the repeatability behavior of cobalt oxide-based system. CuO powders with different particle sizes (i.e. CuO (0.01 M), CuO (0.05 M), and CuO (0.025 M)) were utilized to prepare CuO-doped cobalt oxide composites. The CuO content doped in the composite was

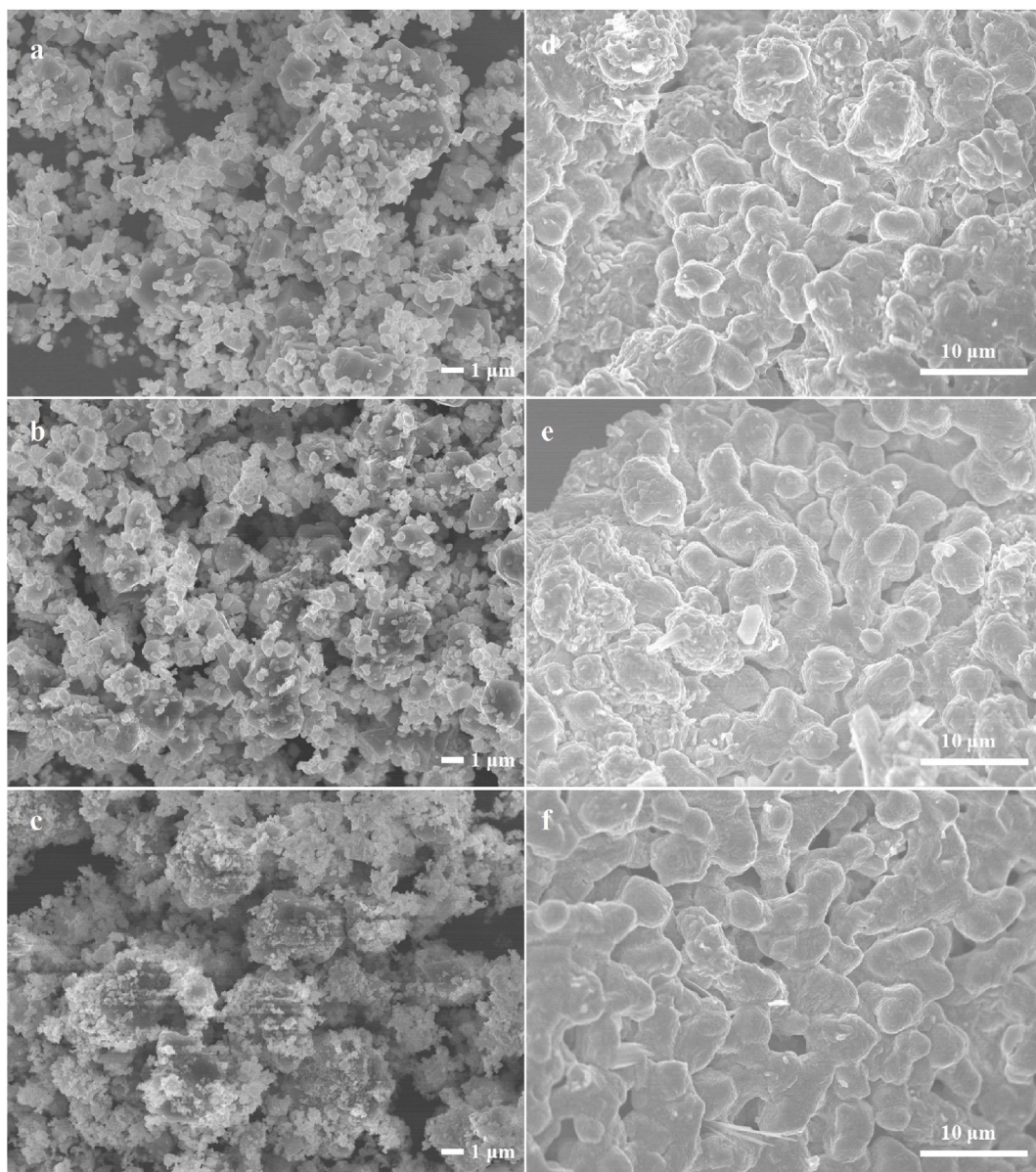


Fig. 13. SEM images taken before and after 30 cycles for composites doped with CuO content of $x = 0.6$: (a and d) CuO (0.1 M)-doped composite, (b and e) CuO (0.05 M)-doped composite and (c and f) CuO (0.025 M)-doped composite.

determined as $x = 0.6$. It is possible to appreciate the different particle sizes of the CuO particles from the SEM images of the fresh composites (Fig. 13(a–c)). In addition, the values corresponding to the redox behaviors of these composites were summarized in Table 2. The composites were tested in 30 reduction-oxidation cycles by TGA with a heating/cooling rate of 10 °C/min. Fig. 12 displays the TGA curves and the evolutions of re-oxidation conversion in 30 cycles for the composites. It can be observed that doping with smaller particle sizes of CuO improved the repeatability by comparing with the performance of the composite doped with CuO (0.5 M) shown in Fig. 9 (d and h). The composites doped with CuO (0.1 M) and CuO (0.05 M) suffered a decrease in the re-oxidation rate, leading to an incomplete re-oxidation in the cooling step from the 14th cycle for the composite doped with CuO (0.1 M) and from the 17th cycle for the composite doped with CuO (0.05 M). Ultimately, $\beta = 0.85$ and $\beta = 0.91$ were obtained after the cooling step of the 30th cycle for the composites doped with CuO (0.1 M) and CuO (0.05 M), respectively. In contrast, the composite doped with CuO (0.025 M) which presented the relatively small particle size of CuO exhibited a stable repeatability performance, reaching a complete re-oxidation in

each cooling step. Moreover, the composite with CuO (0.025 M) content of $x = 0.6$ was subjected to a more extreme cycling experiment. As shown in Fig. S4, the composite still presented an excellent repeatability behavior in 50 cycles.

The SEM images taken after 30 reduction-oxidation cycles for the composites doped with different particle sizes of CuO are shown in Fig. 13. By comparing, the composites with CuO (0.1 M) and CuO (0.05 M) exhibited relatively high densification after the 30 cycles that there were less pores presented, whereas the composite doped with CuO (0.025 M) exhibited more pores after the 30 cycles. Moreover, the composite still presented several open pores after 50 reduction-oxidation cycles (Fig. S4). Particles could be observed hardly from the surface of the bulk for the composite doped with CuO (0.025 M), which might be due to the high degree of coarsening. The result indicates that doping with CuO that presented relatively small particle size might be beneficial for following a coarsening-favorable sintering process, leading to a positive effect on the repeatability performance for CuO-doped cobalt oxide composite.

To date, several directly irradiated solar reactors for metal oxide-

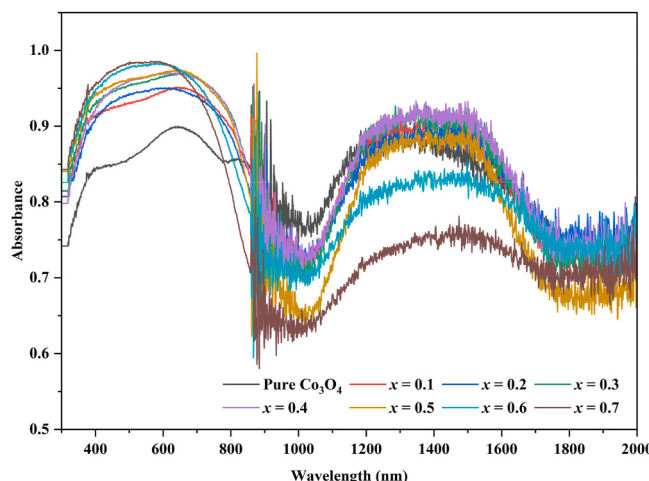


Fig. 14. Absorption spectra of pure cobalt oxide and composite doped with different CuO (0.025 M) contents (x).

based TCS system have been proposed [23,41]. In this case, the optical absorption properties of the energy storage materials are significant. Thus, the composites doped with CuO (0.025 M), which exhibited the best performance in this work were tested by a UV-Visible-NIR-Spectrophotometer. As displayed in Fig. 14, all the composites presented increased absorbance in the wavelength range from 300 nm to 750 nm compared to pure cobalt oxide, revealing that the CuO doping enhanced the absorption of visible light. Moreover, with an increase in CuO doping amount, the absorbance increased slightly. In the wavelength range from 750 nm to 2000 nm, all samples exhibited fluctuating curves which might be related to the relatively large particle size of Co₃O₄. Meanwhile, pure cobalt oxide and the composites with $x \leq 0.4$ showed similar absorbance values, whereas the composites with $x \geq 0.5$ exhibited decreased absorbance in NIR region. Nonetheless, the result demonstrates that the CuO-doped cobalt oxide was feasible for the direct solar radiation absorption.

4. Conclusion

In this work, CuO-doped cobalt oxide composite was prepared by a simple mechanical mixing process for TCS application. Meanwhile, a series of CuO powders with different particle sizes were synthesized by means of precipitation method using different copper nitrate concentrations.

The influence of CuO doping on the redox behavior of cobalt oxide was investigated. Doping with CuO significantly decreased the onset temperature of reduction by 60 °C compared to pure cobalt oxide. Meanwhile, the result verifies that the onset temperature of re-oxidation could be tuned in the range from 825 °C to 890 °C by altering the doping amount of CuO. The structural transformation of CuO-doped cobalt oxide composite during reduction/re-oxidation process was confirmed by in-situ XRD. Moreover, it was found that CuO was involved in the reduction/re-oxidation process of cobalt oxide. Cu species was doped in the CoO structure during the reduction process and separated out during the re-oxidation process. It was presumed that the doping amount of Cu species in CoO might be related to the onset temperature of re-oxidation for the composite.

The effect of CuO doping on the repeatability performance of cobalt oxide was also explored. The result under 30 reduction-oxidation cycles demonstrates that the repeatability of the composite was highly affected by the doping amount of CuO. Deterioration in the repeatability performance was observed with the increase of CuO doping amount. However, it was found that CuO with relatively small particle size exhibited a positive effect on improving the repeatability of CuO-doped cobalt oxide composite.

Additionally, the absorption spectra demonstrate that CuO doping would affect the optical absorption property of the composite, enhancing the absorption of visible light.

Hence, the results obtained in this work indicate that doping with CuO could extend the applicability of cobalt oxide-based system for thermochemical energy storage application.

CRediT authorship contribution statement

Rongjun Wu: Writing – original draft, Methodology, Investigation, Conceptualization. **Hongyu Huang:** Writing – review & editing, Resources. **Lisheng Deng:** Investigation. **Mitsuhiro Kubota:** Investigation. **Noriyuki Kobayashi:** Supervision, Project administration, Funding acquisition.

Declaration of competing interest

The authors declare that they have no known competing financial interests or personal relationships that could have appeared to influence the work reported in this paper.

Data availability

Data will be made available on request.

Acknowledgements

This work was partially supported by “Knowledge Hub Aichi”, Priority Research Project from Aichi Prefectural Government, Japan and the National Natural Science Foundation of China (No.52176091).

Appendix A. Supplementary data

Supplementary data to this article can be found online at <https://doi.org/10.1016/j.solmat.2023.112211>.

References

- [1] N. Kannan, D. Vakeesan, Solar energy for future world: - a review, *Renew. Sustain. Energy Rev.* 62 (2016) 1092–1105.
- [2] A.J. Carrillo, J. Gonzalez-Aguilar, M. Romero, J.M. Coronado, Solar energy on demand: a review on high temperature thermochemical heat storage systems and materials, *Chem. Rev.* 119 (2019) 4777–4816.
- [3] S. Kuravi, J. Trahan, D.Y. Goswami, M.M. Rahman, E.K. Stefanakos, Thermal energy storage technologies and systems for concentrating solar power plants, *Prog. Energy Combust. Sci.* 39 (2013) 285–319.
- [4] L. Andre, S. Abanades, G. Flamant, Screening of thermochemical systems based on solid-gas reversible reactions for high temperature solar thermal energy storage, *Renew. Sustain. Energy Rev.* 64 (2016) 703–715.
- [5] S. Li, H. Huang, X. Yang, Y. Bai, J. Li, N. Kobayashi, M. Kubota, Hydrophilic substance assisted low temperature LiOH-H₂O based composite thermochemical materials for thermal energy storage, *Appl. Therm. Eng.* 128 (2018) 706–711.
- [6] A. Shkatulov, Y. Aristov, Modification of magnesium and calcium hydroxides with salts: an efficient way to advanced materials for storage of middle-temperature heat, *Energy* 85 (2015) 667–676.
- [7] T. Wang, C.Y. Zhao, J. Yan, Investigation on the Ca(OH)₂/CaO thermochemical energy storage system with potassium nitrate addition, *Sol. Energy Mater. Sol. Cell.* 215 (2020), 110646.
- [8] C. Ortiz C., J.M. Valverde, R. Chacartegui, L.A. Perez-Maqueda, P. Gimenez, The calcium-looping (CaCO₃/CaO) process for thermochemical energy storage in concentrating solar power plants, *Renew. Sustain. Energy Rev.* 113 (2019), 109252.
- [9] N. Amghar, C. Ortiz, A. Perejon, J.M. Valverde, L.P. Maqueda, P.E.S. Jimenez, The SrCO₃/SrO system for thermochemical energy storage at ultra-high temperature, *Sol. Energy Mater. Sol. Cell.* 238 (2022), 111632.
- [10] B. Wong, Thermochemical Heat Storage for Concentrated Solar Power, Final Report for the U.S. Department of Energy, United States, 2011, pp. 10–31.
- [11] A. Bayon, R. Bader, M. Jafarian, L. Fedunik-Hofman, Y. Sun, J. Hinkley, S. Miller, W. Lipski, Techno-economic assessment of solid-gas thermochemical energy storage systems for solar thermal power applications, *Energy* 149 (2018) 473–484.
- [12] A.J. Carrillo, D. Sastre, D.P. Serrano, P. Pizarro, J.M. Coronado, Revisiting the BaO/BaO redox cycle for solar thermochemical energy storage, *Phys. Chem. Chem. Phys.* 18 (2016) 8039–8048.

- [13] F. Lei, A. Dyall, N. AuYeung, An in-depth investigation of BaO₂/BaO redox oxides for reversible solar thermochemical energy storage, *Sol. Energy Mater. Sol. Cell.* 223 (2021), 110957.
- [14] A.J. Carrillo, D.P. Serrano, P. Pizarro, J.M. Coronado, Thermochemical heat storage based on the Mn₂O₃/Mn₃O₄ redox couple: influence of the initial particle size on the morphological evolution and cyclability, *J. Mater. Chem. 2* (2014) 19435–19443.
- [15] C. Agrafiotis, M. Roeb, M. Schmucker, C. Sattler, Exploitation of thermochemical cycles based on solid oxide redox systems for thermochemical storage of solar heat. Part 1: testing of cobalt oxide-based powders, *Sol. Energy* 102 (2014) 189–211.
- [16] E. Alonso, C. Perez-Pabago, J. Licurgo, E. Fuentealba, C.A. Estrada, First experimental studies of solar redox reactions of copper oxides for the thermochemical energy storage, *Sol. Energy* 115 (2015) 297–305.
- [17] K.J. Albrecht, G.S. Jackson, R.J. Braun, Thermodynamically consistent modeling of redox-stable perovskite oxides for thermochemical energy conversion and storage, *Appl. Energy* 165 (2016) 285–296.
- [18] Z. Zhang, L. Andre, S. Abanades, Experimental assessment of oxygen exchange capacity and thermochemical redox cycle behavior of Ba and Sr series perovskites for solar energy storage, *Sol. Energy* 134 (2016) 494–502.
- [19] N. Gokon, T. Yawata, S. Bellan, T. Kodama, H.S. Cho, Thermochemical behavior of perovskite oxides based on La_xSr_{1-x}(Mn, Fe, Co)O_{3-δ} and Ba_ySr_{1-y}CoO_{3-δ} redox system for thermochemical energy storage at high temperature, *Energy* 171 (2019) 971–980.
- [20] A.J. Carrillo, D.P. Serrano, P. Pizarro, J.M. Coronado, Understanding redox kinetics of iron-doped manganese oxides for high temperature thermochemical energy storage, *J. Phys. Chem. 120* (2016) 27800–27812.
- [21] F. Varsano, C. Alvani, A.L. Barbera, A. Masi, F. Padella, Lithium manganese oxides as high-temperature thermal energy storage system, *Thermochim. Acta* 640 (2016) 26–35.
- [22] N.W. Hlongwa, D. Sastre, E. Iwuoha, A.J. Carrillo, C. Ikpo, D.P. Serrano, P. Pizarro, J.M. Coronado, Exploring the thermochemical heat storage capacity of AMn₂O₄ (A = Li or Cu) Spinels, *Solid State Ionics* 320 (2018) 316–324.
- [23] M. Neises, S. Tescari, L. de Oliveira, M. Roeb, C. Sattler, B. Wong, Solar-heated rotary kiln for thermochemical energy storage, *Sol. Energy* 86 (2012) 3040–3048.
- [24] M. Wokon, A. Kohzer, M. Linder, Investigations on thermochemical energy storage based on technical grade manganese-iron oxide in a lab-scale packed bed reactor, *Sol. Energy* 153 (2017) 200–214.
- [25] S. Tescari, A. Singh, C. Agrafiotis, L. de Oliveira, S. Breuer, B. Schlögl-Knothe, M. Roeb, C. Sattler, Experimental evaluation of a pilot-scale thermochemical storage system for a concentrated solar power plant, *Appl. Energy* 189 (2017) 66–75.
- [26] S. Álvarez de Miguel, J. Gonzalez-Aguilar, M. Romero, 100-Wh multi-purpose particle reactor for thermochemical heat storage in concentrating solar power plants, *Energy Proc.* 49 (2014) 676–683.
- [27] K.N. Hutchings, M. Wilson, P.A. Larsen, R.A. Cutler, Kinetic and thermodynamic considerations for oxygen absorption/desorption using cobalt oxide, *Solid State Ionics* 177 (2006) 45–51.
- [28] C. Agrafiotis, M. Roeb, M. Schmucker, C. Sattler, Exploitation of thermochemical cycles based on solid oxide redox systems for thermochemical storage of solar heat. Part 2: redox oxide-coated porous ceramic structures as integrated thermochemical reactors/heat exchangers, *Sol. Energy* 114 (2015) 440–458.
- [29] C. Agrafiotis, S. Tescari, M. Roeb, M. Schmucker, C. Sattler, Exploitation of thermochemical cycles based on solid oxide redox systems for thermochemical storage of solar heat. Part 3: cobalt oxide monolithic porous structures as integrated thermochemical reactors/heat exchangers, *Sol. Energy* 114 (2015) 459–475.
- [30] T. Block, N. Knoblauch, M. Schmucker, The cobalt-oxide/iron-oxide binary system for use as high temperature thermochemical energy storage materials, *Thermochim. Acta* 577 (2014) 25–32.
- [31] A.J. Carrillo, J. Moya, A. Bayon, P. Jana, V.A. de la Pena O'Shea, M. Romero, J. Gonzalez-Aguilar, D.P. Serrano, P. Pizarro, J.M. Coronado, Thermochemical energy storage at high temperature via redox cycles of Mn and Co oxides: pure oxides versus mixed ones, *Sol. Energy Mater. Sol. Cell.* 123 (2014) 47–57.
- [32] T. Block, M. Schmucker, Metal oxides for thermochemical energy storage: a comparison of several metal oxide systems, *Sol. Energy* 126 (2016) 195–207.
- [33] L. Andre, S. Abanades, L. Cassayre, High-temperature thermochemical energy storage based on redox reactions using Co-Fe and Mn-Fe mixed metal oxides, *J. Solid State Chem.* 253 (2017) 6–14.
- [34] Y. Portilla-Nieto, A. Zaki, K. Vidal, M. Hernaiz, E. Aranzabe, S. Doppiu, A. Faik, Development of Co_{3-x}Ni_xO₄ materials for thermochemical energy storage at lower red-ox temperature, *Sol. Energy Mater. Sol. Cell.* 230 (2021), 111194.
- [35] W. Stichert, F. Schutth, Influence of crystallite size on the properties of zirconia, *Chem. Mater.* 10 (1998) 2020–2026.
- [36] K. Phiwdang, S. Suphanikit, W. Mekprasart, W. Pecharapa, Synthesis of CuO nanoparticles by precipitation method using different precursors, *Energy Proc.* 34 (2013) 740–745.
- [37] M.W. Hussain, M.Y.H. Ansari, Significance and importance of thermal expansion, *IOSR J. Appl. Phys.* 9 (2017) 68–73.
- [38] Z.Z. Fang, H. Wang, V. Kumar, Coarsening, densification, and grain growth during sintering of nano-sized powders – a perspective, *Int. J. Refract. Metals Hard Mater.* 62 (2017) 110–117.
- [39] X. Wang, A. Atkinson, Combining densification and coarsening in a Cellular Automata-Monte-Carlo simulation of sintering: Methodology and calibration, *Comput. Mater. Sci.* 143 (2018) 338–349.
- [40] R.M. German, Coarsening in sintering: grain shape distribution, grain size distribution, and grain growth kinetics in solid-pore systems, *Crit. Rev. Solid State Mater. Sci.* 35 (2010) 263–305.
- [41] E. Alonso, C. Pérez-Rábago, J. Licurgo, A. Gallo, E. Fuentealba, C.A. Estrada, Experimental aspects of CuO reduction in solar-driven reactors: comparative performance of a rotary kiln and a packed-bed, *Renew. Energy* 105 (2017) 665–673.